International Journal of Applied Earth Observations and Geoinformation 110 (2022) 102789

Contents lists available at ScienceDirect

International Journal of Applied Earth Observations and Geoinformation

journal homepage: www.elsevier.com/locate/jag

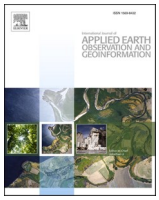

A hybrid spatiotemporal convolution-based cellular automata model (ST-CA) for land-use/cover change simulation

Jiachen Geng [a,b], Shi Shen [a,b,*], Changxiu Cheng [a,b,*], Kaixuan Dai [a,b]

[a] State Key Laboratory of Earth Surface Processes and Resource Ecology, Beijing Normal University, Beijing 100875, China
[b] Faculty of Geographical Science, Beijing Normal University, Beijing 100875, China

ARTICLE INFO

Keywords:
Land-use change
Simulation
Spatiotemporal modeling
Nonlinear process
Three-dimensional convolution
Cellular automata

ABSTRACT

Accurate land-use/-cover change (LUCC) simulation is of great significance to issues closely related to regional planning and policy-making. Many models have been committed to conducting LUCC simulations for better decision-making. However, LUCC is a nonlinear spatiotemporal process with complex links and feedback as well as latent dependencies in both spatial and temporal neighborhoods. They are challenging to be integrally utilized using existing models that employ conventional statistical or machine learning methods, inevitably leading to inaccurate LUCC simulations. Aiming to handle this problem, this paper innovatively proposed a hybrid spatiotemporal convolution-based cellular automata model (ST-CA) by coupling nonlinear spatiotemporal dependency learning and CA-based spatial allocation. A three-dimensional convolutional neural network (3D-CNN) was introduced in the model to assimilate both the nonlinear driving mechanism and spatiotemporal dependencies. It contributes to generating more elaborate development potentials to increase simulation accuracy. To evaluate the model performance, an LUCC simulation was applied on a national scale in China by ST-CA. Four traditional CA models, namely, logistic regression (LR)-CA, random forest (RF)-CA, full-connected neural network (FCN)-CA, and convolutional neural network (CNN)-CA, were also developed for accuracy comparisons. The results demonstrate that the simulation by ST-CA reached an FoM of 18.42%, which outperformed the other models with accuracy increases of 11.65%, 13.11%, 7.01%, and 2.29%, respectively. The proposed model incorporating 3D-CNN effectively captured the nonlinear spatiotemporal properties in the LUCC process, which is promising for more accurate LUCC simulations.

1. Introduction

Land-use/cover change (LUCC) reflects the renovation and utilization of the Earth's surface by human activities (Y. Liu et al., 2014). It is closely related to issues concerning sustainable development, such as carbon neutrality, climate change, ecological restoration, and disaster prevention (K. Cao et al., 2012; Houghton & Nassikas, 2017; G. Li et al., 2017; Shafizadeh-Moghadam et al., 2019). LUCC models are effective tools to support the analysis of the causes and consequences of land-use dynamics (Verburg et al., 2004).

Cellular automata (CA)-based models are among the most remarkable algorithms for conducting LUCC simulations due to their spatial explicitness and dynamic principles (X. Liu et al., 2017; Yao et al., 2017). However, pure CA models merely consider the immediate interactions between land use cells rather than the driving relationship between LUCC and external factors, which leads to unconvincing simulations in practice (Vani & Prasad, 2021). Thus, developing hybrid models integrating CA with other modeling methods to apply multiple concepts of different approaches has become a preferable strategy (Anurag et al., 2018). Numerous studies have indicated that hybrid models incorporating smarter algorithms outperform pure CA models on multiple regions and scales (Kourosh Niya et al., 2020; Mishra et al., 2018; Mustafa et al., 2017; Sankarrao et al., 2021; Vani & Prasad, 2021). Thus, hybrid CA models continue to receive considerable attention and remain one of the most appropriate techniques for LUCC simulations (Sante et al., 2010; Vani & Prasad, 2021).

Within the hybrid CA-based models, the generation of transition rules and the allocation of land cells are the two crucial parts(M. Cao et al., 2015; Y. Feng & Tong, 2018). Although different CA models provide variant spatial allocation approaches, which may lead to

* Corresponding authors at: State Key Laboratory of Earth Surface Processes and Resource Ecology, Beijing Normal University, Beijing 100875, China. State Key Laboratory of Earth Surface Processes and Resource Ecology, Beijing Normal University, Beijing 100875, China.
E-mail addresses: shens@bnu.edu.cn (S. Shen), chengcx@bnu.edu.cn (C. Cheng).

https://doi.org/10.1016/j.jag.2022.102789
Received 9 January 2022; Received in revised form 4 April 2022; Accepted 13 April 2022
Available online 10 May 2022

manifold simulations of landscape dynamics, the proper calculation of development potentials is the key to implementing more accurate LUCC simulations (Xing et al., 2020). These potentials embody alternative future landscape dynamics related to both socioeconomic and natural environmental factors, which are essential driving forces for land-use transition (Verburg et al., 2004).

However, precise development potentials are challenging to generate consummately (Shafizadeh-Moghadam et al., 2017). LUCC is a nonlinear process that contains complex linkages and feedbacks between land use and driving forces (Schulp et al., 2008). Statistical models, such as logistic regression, struggle to comprehensively analyze the driving mechanism of LUCC due to concise structures and intuitive parameters (Ding et al., 2013; Gharaibeh et al., 2020), especially in large areas with complex human-environment relationships. To overcome this obstacle, some researchers have adopted machine learning (ML) methods, such as random forest (RF) (Liang et al., 2021), support vector machine (SVM) (Rienow & Goetzke, 2015; Mustafa et al., 2018), and artificial neural networks (ANNs) (Gharaibeh et al., 2020; Rahman & Esha, 2020), to better express the nonlinear mechanism.

Moreover, LUCC is a dynamic geographical process that involves complex spatiotemporal dependencies (He et al., 2018; J. Liu et al., 2014; Sidharthan & Bhat, 2012). The conversion of a target land cell is affected by both spatial correlation and temporal dependency. Spatial correlation can be regarded as the tendency that closer pixels exert more influence on the target cell compared with further pixels (Shafizadeh-Moghadam et al., 2017), which is a manifestation of Tobler's first law of geography (Tobler, 1970). Temporal dependency refers to the inertia between time units, which means that the future land-use type is influenced by its past attributes (Xing et al., 2020). For example, unused land can hardly be converted to forest without an extended accumulation period irrespective of human interference.

Previous studies have made many efforts to address spatiotemporal dependencies. For the spatial correlations, current practices are mostly confined to expressing the numerical proportion of a specific land-use type in neighbors, which are still insufficient to handle the complex spatial heterogeneity (X. Liu et al., 2018). A more consummate method is to extract the latent spatial features by using convolutional neural networks (CNNs), which helps to achieve more accurate simulations in CA-based models (Ma et al., 2018; Y. Zhai et al., 2020). However, temporal dependencies have still not received much attention and are inadequately expressed in LUCC modeling. Prevalent methods, including LR, RF, SVM, and ANN, essentially regard LUCC as a Markov process, which assumes that the current state of a given land cell is related only to its last time step but is unrelated to its extended history (Gounaridis et al., 2019; Grekousis, 2019). Although some ML methods have been introduced to utilize long-term temporal features, e.g., recurrent neural networks (RNNs) (C. Cao et al., 2019; He et al., 2018) and long short-term memory networks (LSTMs) (Xing et al., 2020), they focus only on extracting temporal features from land-use maps rather than assimilating the relationship between the sequence of driving factors and the land-use situation. Furthermore, the joint utilization of spatiotemporal properties in the LUCC process is not convincing enough in these models. A key problem is that the spatial correlations and the temporal dependencies are separately processed in these methods, but it is difficult to determine which effect is dominant or whether it is credible to handle it one after another. Thus, existing studies inevitably omit the coupling effects in the spatiotemporal LUCC process, which leaves room for further improvements.

To tackle the above deficiencies, we propose a hybrid spatiotemporal convolution-based cellular automata model (ST-CA) coupling spatiotemporal property learning and CA-based spatial allocation. It employs a potential generation module using a three-dimensional convolutional neural network (3D-CNN) to calculate the development potentials of each cell and a spatial allocation module using a patch-based CA to simulate the future LUCC. The proposed model was expected to utilize the spatiotemporal neighborhood properties integrally for a more accurate LUCC simulation.

To evaluate the performance of the ST-CA model, we carried out an LUCC simulation of China from 2010 to 2015 on a national scale. Four statistical or machine learning (ML)-based models, namely, logistic regression (LR)-CA, random forest (RF)-CA, fully connected neural network (FCN)-CA, and convolutional neural network (CNN)-CA, were simultaneously applied to the same dataset to facilitate model comparison.

The remainder of this paper is organized as follows. Section 2 introduces the model framework, principle, parameters, and data source. Section 3 presents the simulation results and compares the models. Section 4 is the discussion where we address our strengths and weaknesses. Finally, Section 5 ends with conclusions.

2. Methodology

2.1. The ST-CA model framework

The ST-CA model is a hybrid model simulating LUCC by integrally utilizing both the spatial and temporal neighborhood properties of driving factors. The framework of the model is shown in Fig. 1. It consists of two main modules, namely, the potential generation module and the spatial allocation module. The potential generation module employs a 3D-CNN to calculate the development potential for every land-use type of each pixel. The spatial allocation module uses the potential maps to explicitly simulate land-use change based on the given land demands. The training and validation sets are required to train the model, while the testing set, land demands, and initial map are used for prediction.

2.1.1. Potential generation module: Employing 3D-CNN to assimilate spatiotemporal properties

The transition of a land-use cell is affected by its spatiotemporal neighborhoods (Milad et al., 2016). Meanwhile, the nonlinear driving mechanism is mingled in the spatiotemporal process, which makes it more difficult to comprehensively interpret (Ju et al., 2016). Here, we introduce the 3D-CNN to assimilate both the spatiotemporal properties and the nonlinear mechanism during the LUCC process.

The 3D-CNN is a neural network algorithm first adopted for motion detection and prediction in digital video processing (Ji et al., 2013). It is able to capture both the spatial correlation and temporal dependency of neighborhoods (Tran et al., 2015) and to express the nonlinear driving mechanism of the LUCC process. It extends the convolution operation to the time dimension to extract mutual information between adjacent video frames. LUCC, representing the spatiotemporal dynamics of land-use patterns to a certain extent, can be regarded as a specific kind of motion. Thus, predicting future LUCC is analogous to dealing with a classification problem from a geographical point of view. Specifically, every pixel is endowed with spatial significance such that the central pixels are influenced by natural and human activities in their vicinities. The map of driving factors and land use at several time slices can be regarded as the frames that depict the evolution of geographical processes. Meanwhile, the connections between neurons help to interpret the nonlinear driving mechanism within the LUCC process. Hence, 3D-CNN is eligible to generate the development potentials of each pixel to become each land-use type taking both the spatiotemporal effects and the nonlinear relationship into account.

Theoretically, the 3D-CNN is an extension of a 2D-CNN with an extra dimension, i.e., time (Tran et al., 2015). The formation of 3D convolution is illustrated in Fig. 2 by comparing it with the conventional 2D convolution. In a 2D-CNN, convolutions are applied to the two spatial dimensions. The driving factors are loaded into different channels. Latent features can be extracted by sliding the distinct kernels throughout the multichannel plane (Ji et al., 2013). In the 3D-CNN, convolutions are simultaneously applied to both the spatial dimensions and the temporal dimension. It convolves a 3D kernel to the cube formed by stacking multiple contiguous frames together, which

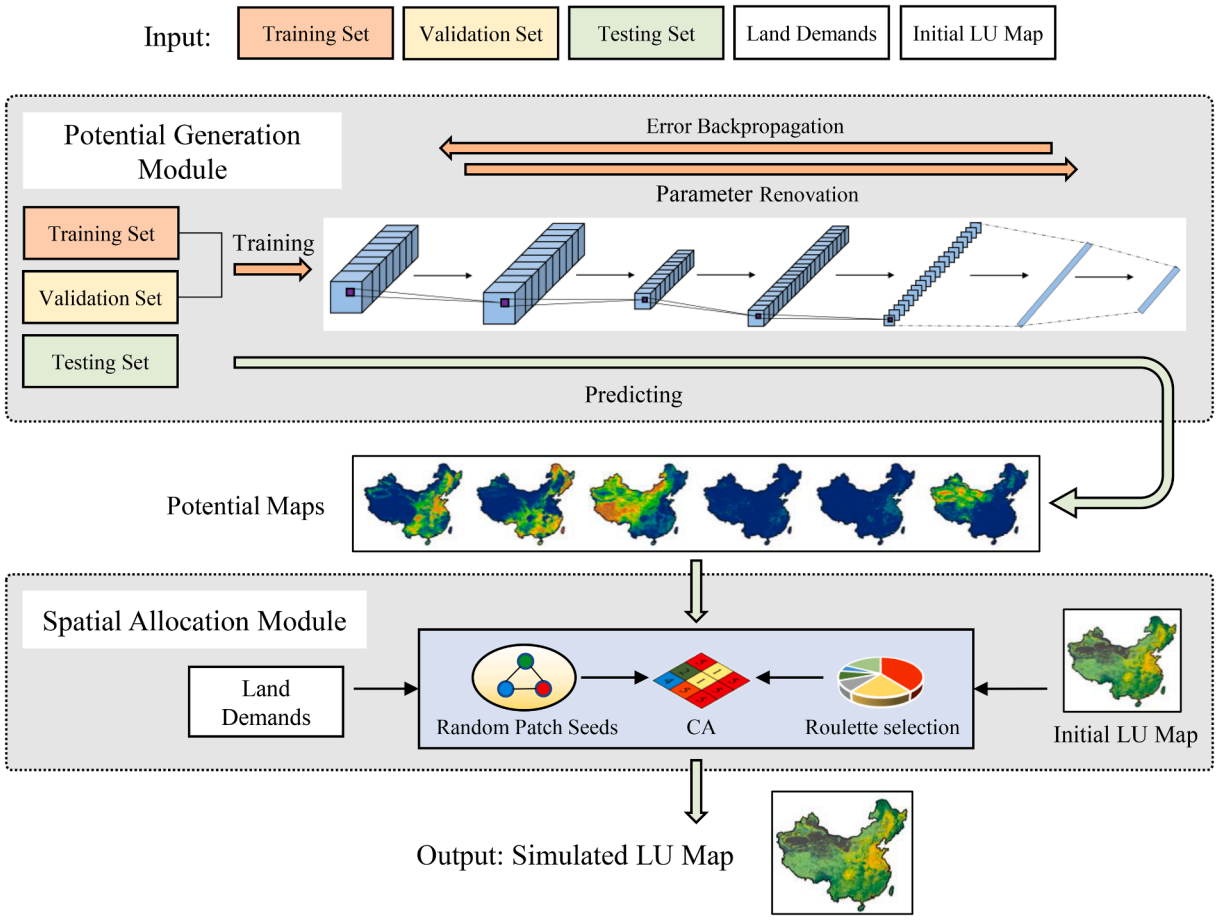

Fig. 1. Framework of the ST-CA model.

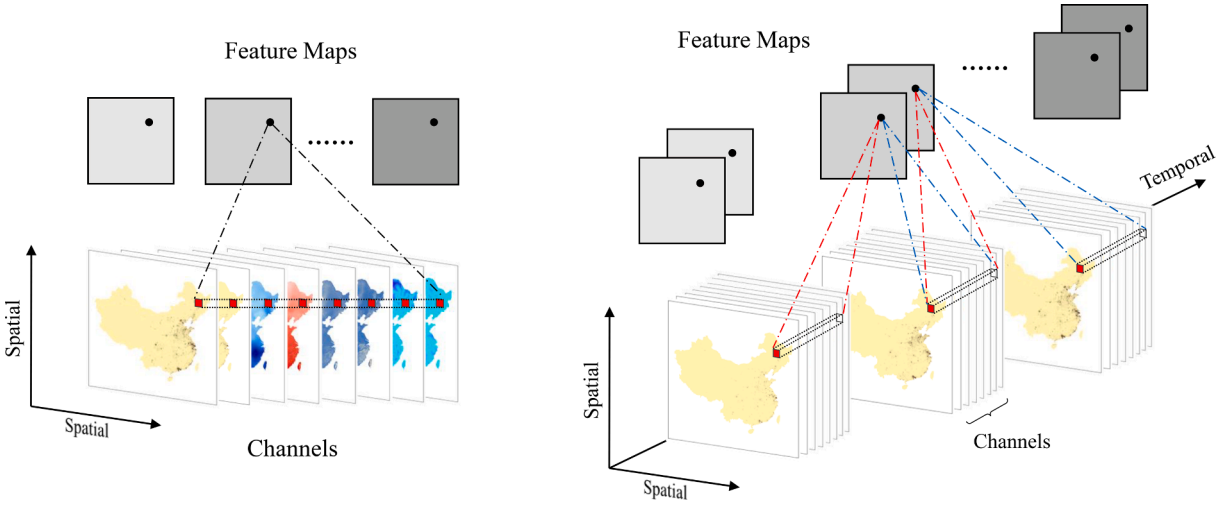

Fig. 2. Illustration of (a) 2D convolution and (b) 3D convolution. Dashed lines in the same color denote shared parameters.

means that the feature maps in the convolution layer are connected to multiple contiguous frames in the previous layer. Analogous to the 2D-CNN, the driving factors of a time slice are loaded into different channels of a single frame. Kernels slide on and between the frames to create new space–time cubes.

Formally, the elementary 3D convolution operation, which generates the value of a unit at position (x, y, z) in the j th feature map of the i th layer, is denoted as v_{ij}^{xyz} and is given by Eq. (1),

$$v_{ij}^{xyz} = \sigma\left(b_{ij} + \sum_{m}\sum_{p=0}^{P_i-1}\sum_{q=0}^{Q_i-1}\sum_{r=0}^{R_i-1} w_{ijm}^{pqr} v_{(i-1)m}^{(x+p)(y+q)(z+r)}\right) \quad (1)$$

where $\sigma(\bullet)$ represents the activation function; b_{ij} is the bias item; m represents the set of feature maps in the $(i-1)$ th layer connected to the current feature map; P_i, Q_i, and R_i are the height, width, and time slide of the kernel, respectively; and w_{ijm}^{pqr} is the (p, q, r) th value of the kernel connected to the m th feature map in the previous layer.

In this paper, we constructed a 3D-CNN with the structure presented in Fig. 3. It consists of 7 layers, including an input layer, 2 convolutional layers, 2 max-pooling layers, a fully connected layer, and an output layer. The input layer was defined as a cube with 3 time slices, 8 channels (8 driving factors), and an 11 × 11 spatial window in consideration of the practical significance, data accessibility, and computational efficiency. Then, it was successively followed by a 3D convolutional layer consisting of 10 kernels of 5 × 5 × 2, a 3D max-pooling layer of 2 × 2 × 1, a 3D convolutional layer consisting of 20 kernels of 3 × 3 × 2, a 3D max-pooling layer of 2 × 2 × 3, a fully connected layer containing 100 neurons, and a layer containing 6 neurons outputting the probabilities that the input cube be classified to each category by a SoftMax function. In addition, a dropout rate of 0.25 was set to the fully connected layer to prevent overfitting.

2.1.2. Spatial allocation module: A CA package based on multiple random patch seeds.

CA-based models have been extensively employed in LUCC simulations (S. Li et al., 2017; X. Liu et al., 2017). They discretely allocate land pixels at the grid cell level in terms of time and space and hence are adept at representing the spatiotemporal processes of LUCC (Xing et al., 2020). The CA based on multiple random patch seeds for space allocation (CARS), first developed in the patch-generating land-use simulation (PLUS) model (Liang et al., 2021), was employed in this study as the spatial allocation module. It integrates both 'top-down' and 'bottom-up' processes and is reputed to generate more realistic spatial structures by its flexible patch-based strategies for multiple land-use types at a fine-scale resolution. This CA module, which is based on multiple random patch seeds and roulette selection, was found to be remarkable for accurately simulating the LUCC on multiple scales (C. Li et al., 2021; Liang et al., 2021; M. Shi et al., 2021; H. Zhai et al., 2021).

The inputs of the CARS mainly include the initial land-use pattern, development potential, and land demand. Generally, the initial map refers to the actual land use of the start year, and the land demands specify the amount of each land-use type in the target year. In the simulation process, the land demands are explicitly allocated to the entire region according to the initial map and development potentials. A local land-use competition mechanism through a self-adaptive coefficient drives the amount of land use to reach future demands. It has been proven to be able to accurately simulate LUCC on multiple scales. Thus, the CARS was connected with the potential generation module to formulate the hybrid ST-CA model to simulate future LUCC.

2.2. Other hybrid models developed for comparison

To illustrate the advancement of ST-CA, other hybrid models (i.e., LR-CA, RF-CA, FCN-CA, and CNN-CA) were developed for accuracy comparison. Among the existing methods, LR, RF, FCN, and CNN, which partially consider the spatiotemporal dependency or nonlinear effects, are prevalent methods to establish the driving mechanism of LUCC. In this study, LR-CA, RF-CA, FCN-CA, and CNN-CA were constructed to form the same structure as ST-CA for comparison. They all shared the same spatial allocation module, but the potential generation modules were replaced by the methods mentioned above.

As a conventional statistical method, LR is based on the log-linear expression given by Eq. (2).

$$\log\left(\frac{P_i^k}{1-P_i^k}\right) = \beta_0^k + \sum_{n=1}^{N} \beta_n^k X_{n,i} \tag{2}$$

where P_i^k represents the development potential of cell i to become land-use type k, $X_{n,i}$ is the n th driving factor of cell i, and β_n^k is its coefficient.

The RF employed in this paper consists of 10 decision trees with the max features set to 5 to avoid overfitting. The voting of trees generated the potentials.

As an ANN method, the FCN consisted of 2 I/O layers and 2 hidden layers of 100 neurons each. The dropouts of the hidden layers were set to 0.25 to avoid overfitting.

The CNN (Fig. 4) consisted of 2 convolutional layers, 2 pooling layers, and 2 fully connected layers, which is designed similarly to the 3D-CNN for ease of comparison.

2.3. Model applications and comparisons

To examine the effectiveness of the ST-CA model in complex natural and social environments, we carry out an LUCC simulation of China on a national scale from 2010 to 2015. The flow chart for model application and comparison is illustrated in Fig. 5. Primarily, the land use in 2010 and the driving factors in 2000, 2005, and 2010 were sampled to the proper formation to train the ST-CA. Then, the land demand in 2015 and the factors in 2005, 2010, and 2015 were used to drive the model. Additionally, these data were also fed into the comparison models to obtain other simulations. Finally, accuracy assessments were carried out to compare the model performance. The data sources and model operations are introduced in detail in the following paragraphs.

2.3.1. Data sources and preprocessing

The data used in this study, which consisted of land use, environmental data, and socioeconomic data, are listed in Table 1. Land-use maps of China in 2010 and 2015 with a spatial resolution of 1 km were collected from the Resource and Environment Science and Data Center, and these maps consisted of 6 primary land-use types, namely, arable land, forest, grassland, water, construction land, and unused land. Both environmental and socioeconomic factors influence LUCC. In this paper, 8 factors were selected to drive land-use change in the study period. The environmental data include elevation, annual precipitation, and average annual temperature, while the socioeconomic data include the gross domestic product (GDP), population density, highways, and railways. Elevation, slope, distance to highways and railways were deemed constant during the study period subject to the availability of the data sources. Finally, all the data were normalized and resampled to 1 km grids.

2.3.2. Sampling for training and validation

Samples were generated before training the 3D-CNN in the potential generation module. To address the spatial-decay effect, we used an 11 × 11 sized spatial window (i.e., the central pixel is affected by its 10 km radius neighborhood with a 1 km resolution) considering the trade-off between detail abundance and computational efficiency.

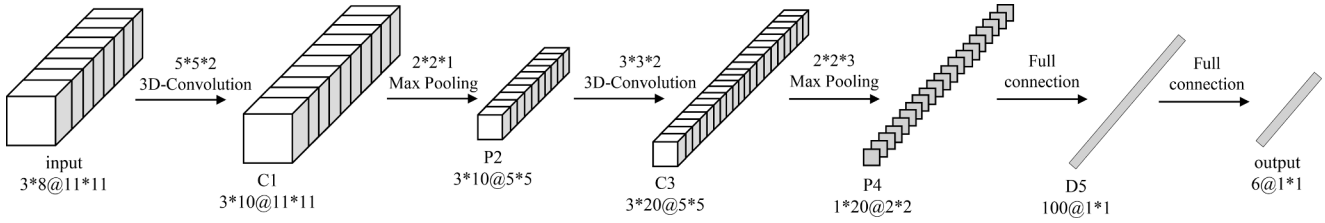

Fig. 3. The structure of the 3D-CNN in the potential generation module.

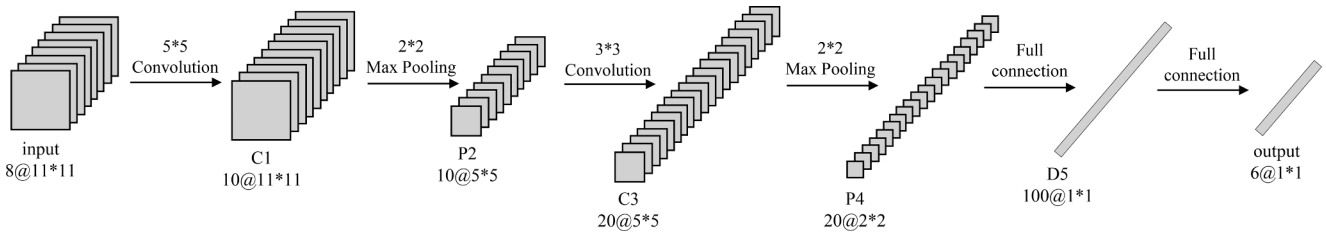

Fig. 4. The structure of the 2D-CNN.

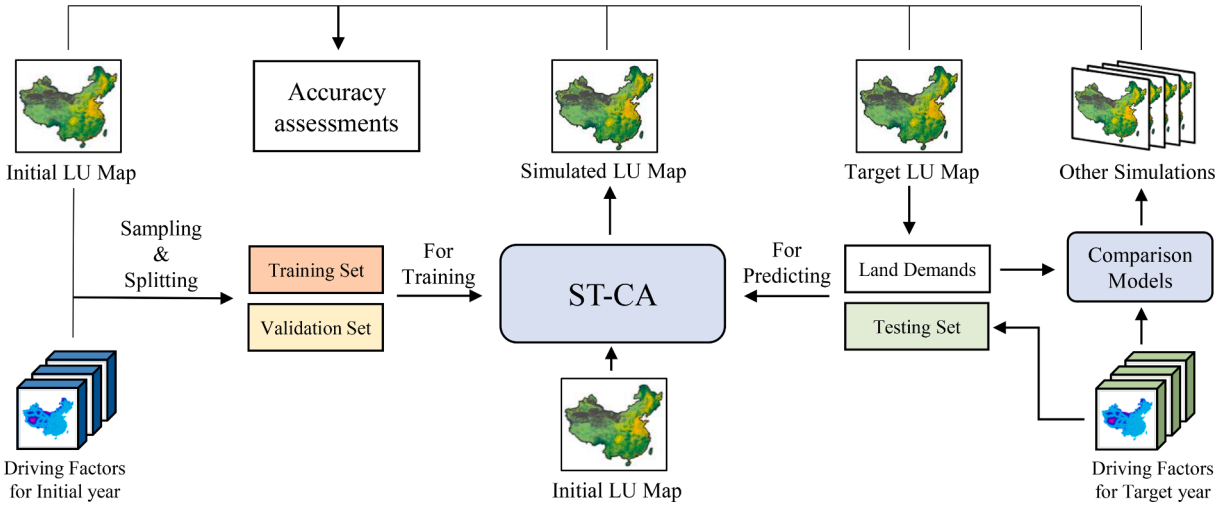

Fig. 5. The flow chart for model application and comparison.

Table 1
Data used in this study.

Data	Variable	Description	Resource
Land-use/cover map	y	1 km raster, 6 primary types, year of 2010, 2015	https://www.resdc.cn
Elevation	X_1	1 km raster, mapping by SRTM in 2000	https://www.resdc.cn
Slope	X_2	1 km raster, calculated in ArcGIS with elevation	–
Temperature	X_3	1 km raster, year of 2000, 2005, 2010, 2015	https://www.resdc.cn
Precipitation	X_4	1 km raster, year of 2000, 2005, 2010, 2015	https://www.resdc.cn
GDP	X_5	1 km raster, year of 2000, 2005, 2010, 2015	https://www.resdc.cn
Population	X_6	1 km raster, year of 2000, 2005, 2010, 2015	https://www.resdc.cn
Distance to Highways	X_7	1 km raster generated in ArcGIS from vectors mapped in 2010	https://www.webmap.cn
Distance to Railways	X_8	1 km raster generated in ArcGIS from vectors mapped in 2010	https://www.webmap.cn

Factor arrays were sampled to cubes in the shape of $3 \times 8 \times 11 \times 11$. For the training process, the driving factors in 2000, 2005, and 2010 were concatenated to an 8-channel array with 3 time slices. The land-use types of the central pixels of the spatial windows in 2010 were selected as training tags. A uniform sampling strategy at intervals of 6 pixels was adopted to obtain an adequate dataset. Finally, a total of 246,108 samples were collected after dropping the no-data samples. The train-test split coefficient was set to 0.2, which means that 80% of the samples were randomly selected as the training set, while the remaining 20% were used for validation. The training set was used to optimize the network weights of the potential generation module using the back-propagation (BP) method, and the validation set was used to examine the network performance after each training epoch.

2.3.3. *Simulating the future LUCC*

Two main steps are required to accomplish an LUCC simulation using the ST-CA model, namely, generating the development potentials and conducting the spatial allocation.

For potential generation, the 3D-CNN was first trained to converge using the training and validation sets with an initial learning rate of 0.001. Then, the trained network was used to predict the development potentials for the target year. The input cubes for prediction were cut to the same size as the training samples from the neighborhood of every location of the 8 driving factors in 2005, 2010, and 2015, which is regarded as the testing set of this study.

For the spatial allocation, the initial land-use pattern, development potential, land demand, and other adjustable parameters are set before running the allocation module. The initial land-use pattern was set based on the actual land-use map in 2010. The demand of each land-use type was set to the actual area in 2015. The spatial allocation procedures were conducted from 2010 to 2015 using the development potentials generated by the 3D-CNN. Parameter tuning was conducted during simulation to obtain the best accuracy.

2.3.4. *Indicators for accuracy evaluation*

An accuracy evaluation was conducted to quantify the performance of the model. For a comprehensive assessment, two indicators were calculated for each of the five hybrid models by comparing the LUCC simulations with the observed maps. From the perspective of conversion accuracy, the figure of merit (FoM) is widely used in LUCC accuracy evaluation and is calculated by Eq. (3):

$$FoM = \frac{H_1}{H_1 + H_2 + M + F} \times 100\% \quad (3)$$

where H_1 represents true hits, which are the correct simulated area; H_2 denotes the partial hits, which is the area of inaccurate prediction due to observed change predicted as the wrong gaining category; M indicates misses, corresponding to areas that actually changed but are simulated as unchanged; and finally, F denotes the false alarms, corresponding to areas that have not changed but are simulated as changed. The FoM ranges from 0% to 100%, and a higher value represents a better prediction of land-use changes.

Furthermore, from the perspective of overall similarity, confusion matrices are employed to quantitively evaluate the consistency between the predicted map and the observed map. The commission error (CE) and the omission error (OE) are calculated to assess underestimations and overestimations, respectively. The CE is the proportion of pixels that are predicted as one category but actually belong to other categories, and OE the is the proportion of pixels in one category but are wrongly predicted as other categories. The kappa coefficient is calculated using formula (4):

$$Kappa = \frac{p_o - p_e}{1 - p_e} \quad (4)$$

$$p_o = \frac{\sum_{i=1}^{m} c_i}{n}$$

$$p_e = \frac{\sum_{i=1}^{m} a_i \times b_i}{n \times n}$$

where i represents the land-use type, c is the number of identical pixels between observation and prediction, a_i is the number of pixels of type i in the observed map, b_i is the number of pixels of type i in the simulated map, and n is the total number of pixels. The kappa coefficient ranges from −1 to 1, and a higher value represents a higher overall similarity.

3. Result

3.1. Generated development potential maps

The development potential of each land-use type generated by the potential generation module in the ST-CA model is shown in Fig. 6, by which the spatial distributions of land use in China were faithfully depicted. For arable land, the regions with high potentials are mainly located in the Songnen Plain, Sanjiang Plain, North China, and Sichuan Basin. For the forest, the high-potential areas locate in the northeast, southwest, and southeast, which are consistent with the three major Chinese forest regions. For grassland, Xilin Gol and Hulunbuir of Inner Mongolia and the Tibetan Plateau are the most suitable regions for development. Water is mainly distributed in southern China and the Tibetan Plateau. Construction land is consistent with developed urban areas. Unused land is mainly distributed in the deserts of the northwest as well as the mountains and valleys of the Tibetan Plateau.

The potential maps generated in the ST-CA are preferable to those generated by other models. As shown in Appendix A1., the LR method generated more evenly distributed potentials because of its linear properties. The RF functions by the voting of multiple decision trees (Breiman, 2001). This resulted in generating discrete probabilities that were not exact enough for accurate LUCC simulations. The FCN and CNN generated smooth potential maps that capture the nonlinear driving mechanism in LUCC, but they were not as precise as those calculated by 3D-CNN. In general, the 3D-CNN has the advantage of assimilating both the nonlinear driving mechanism and spatiotemporal dependencies, which yields a more accurate LUCC simulation.

3.2. Land-use/land-cover simulation and comparison

3.2.1. Spatial pattern of simulations

The simulation results of the ST-CA model and the other comparison models are shown in Fig. 7. A densely populated urban area in the east and a grassland-unused land ecotone in the northwest were selected to compare the details.

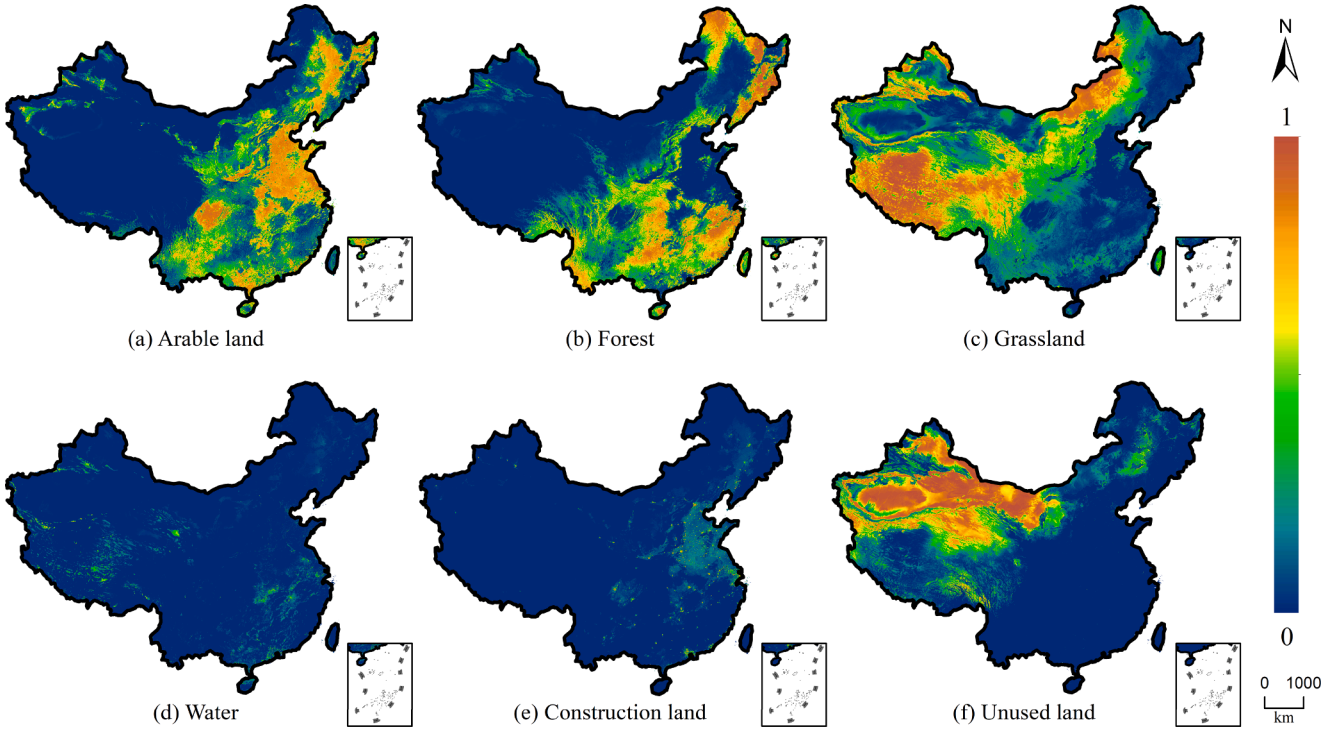

Fig. 6. Potential maps generated by 3D-CNN in the ST-CA model.

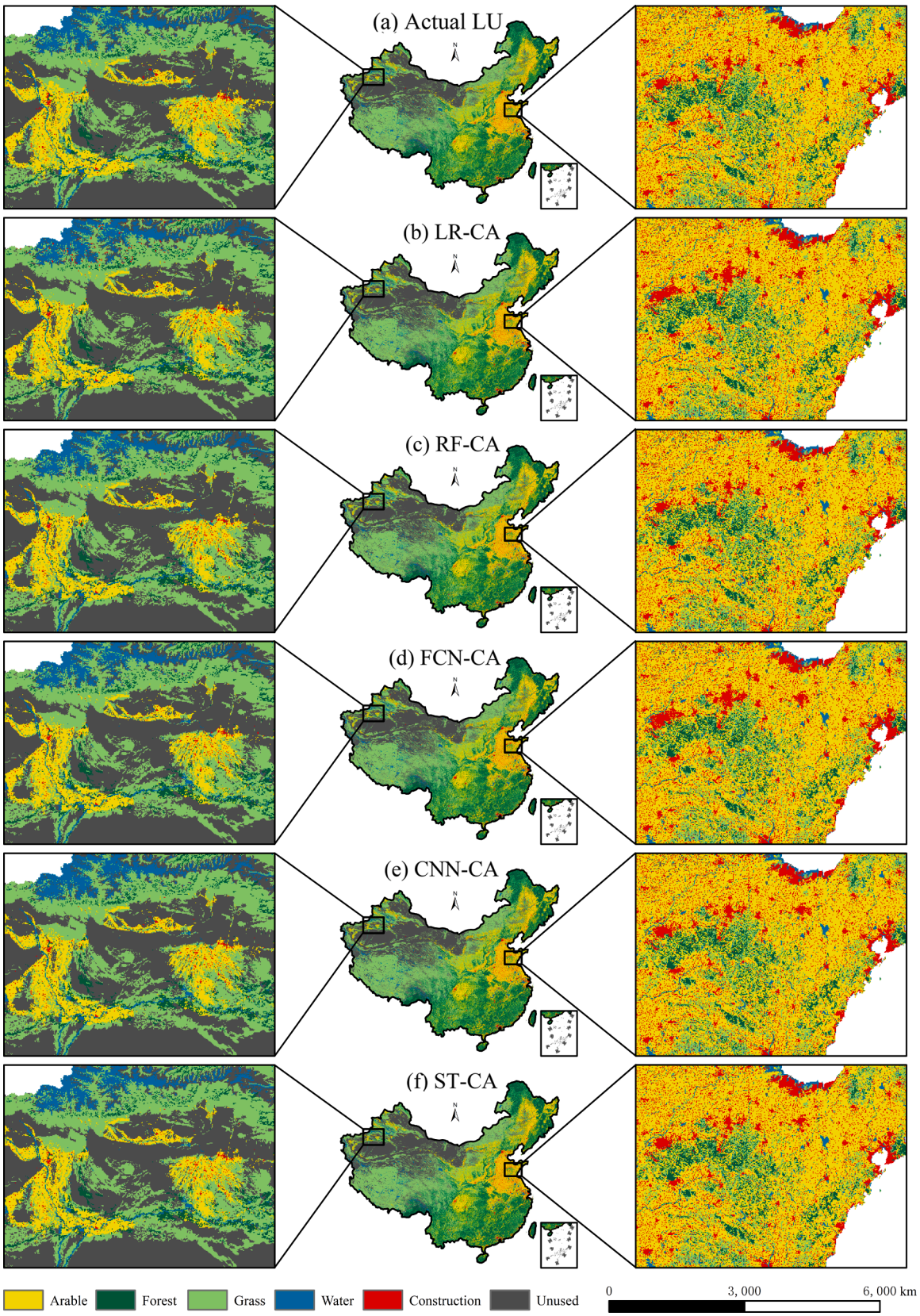

Fig. 7. Comparison between actual land use and simulated results. (a) Actual land-use map of 2015, (b)–(f) simulation results of the ST-CA model and other comparison models.

The overall land-use patterns simulated by the five models are generally in accordance with the actual conditions, which proves the simulation capability of the models. As shown in Fig. 7, the patches simulated by LR and FCN tend to be clumpier, which means that the separated cells merge into integral ones. This trend can be clearly seen in eastern China, where gross overestimation occurred for construction land. The land use simulated by RF exhibits a fragmented pattern resulting from discrete potentials. This leads to an underestimation of the LUCC, where the simulated change is less than the actual change. In contrast, CNN-CA and ST-CA significantly mitigated these biases and were able to reveal more details.

3.2.2. Accuracy comparisons.

An accuracy comparison was conducted to quantitatively illustrate the model performances. The simulation accuracies in 7 subregions of China, namely, Central China (CC), Eastern China (EC), Northern China (NC), Northeastern China (NE), Northwestern China (NW), Southern China (SC), and Southwestern China (SW), were calculated to compare the model performance in the regions with different endowments. Two indicators, namely, the FoM and the kappa, are shown in Table 2. In general, the simulation accuracy in sequence from high to low is ST-CA, CNN-CA, FCN-CA, LR-CA, and RF-CA.

The ST-CA obtains the greatest FoM and kappa in both the subregions and the whole country. Its overall FoM and kappa reached 18.42% and 0.991, respectively. Thus, the FoM of the ST-CA was 11.65% and 13.11% better than those of the LR-CA and RF-CA and 7.01% and 2.29% better than those of the two ANN-based models. Meanwhile, the ST-CA model also achieved the best accuracy in each subregion, yielding an FoM that was higher by 1%–16% and a kappa that was higher by 0–0.011. This demonstrates that the proposed ST-CA can effectively utilize spatiotemporal neighborhood properties and address complex heterogeneities on a national scale. Regionally, the FoM of ST-CA was highest in CC (21.70%) and lower in SW (16.49%). In addition, compared with the CNN-CA model, the ST-CA model improved the FoM of EC by the largest margin (4.03%), indicating that the model is more effective in using the temporal characteristics of land-use change in northeastern China.

In addition, the CE, OE, and total errors of each model for different land-use types were calculated based on the confusion matrices. As shown in Table 3, the ST-CA obtained the least total error of 0.71% among the five models, which is 0.07%-0.17% less than those of the rest. This illustrates that the ST-CA outperformed the other models in terms of predicting the overall patterns of LUCC. For the CE and OE, there is no significant distinction between models because of the relatively sparse changing pixels compared with the extensive study region. Despite this, the proposed ST-CA still obtained the lowest CE for forest (0.16%), water (1.48%), and construction land (7.25%) and the lowest OE for forest (0.23%), water (0.81%), construction land (6.40%), and unused land (0.43%), which accounted for more than half of all land-use types.

Furthermore, it can be seen that the construction land is challenging to be accurately predicted, but ST-CA reduces the most errors on none other land-use types than construction land. It achieves a 0.18%-2.45% decrement on CE and a 0.23%-3.29% decrement on OE. Based on the above evaluation, the ST-CA is the best predictor among the five models, which shows great potential for further application. In addition, detailed information about the confusion matrices is available in Appendix A2.

3.2.3. Error distribution

The spatial distributions of the incorrectly predicted pixels and accurately predicted pixels are mapped in Fig. 8. The whole country was divided into 100 km side-length grids, and the factors of the FoM, namely, false alarms (FA), misses (MS), partial hits (PH), and true hits (TH), were plotted. The predictions in the east are more accurate than those in the west. Spatially, FA are mostly distributed in the Kunlun Mountains in southern Qinghai and urban areas in the North China Plain, and MS are mostly distributed in the northeast, northwest, and southwest. These areas are either alpine regions and deserts with poor climate conditions or rapidly urbanizing regions with complex human-land relationships, where it is more difficult to implement accurate LUCC simulations (Ren et al., 2019). Based on Hu's line as the boundary, the TH are higher in the east, which indicates that it is easier to conduct accurate LUCC simulations in developed regions with dense populations, prosperous economies, and infrastructure, where the independent variable contains a larger amount of information.

The quantitative distributions of FA, MS, PH, and TH of each model are demonstrated in Fig. 9. The five groups of cumulative histograms represent the error proportions of LR-CA, RF-CA, FCN-CA, CNN-CA, and ST-CA. In each group, the darker-colored bar on the top represents all of China, and the 7 lighter-colored bars from top to bottom represent CC, EC, NC, NE, NW, SC, and SW. Evidently, the proportions of TH increase when the model becomes more complicated. However, the FA and MS become variational. Compared with LR-CA and RF-CA, FCN-CA raises the value of FoM by decreasing the MS while FA remain approximately the same. For CNN-CA, even though the proportions of FA are larger than those of the other models, the significant reductions in MS improve the FoM. For the best-performing ST-CA, the amounts of FA and MS simultaneously decrease, resulting in the highest accuracy among the five models. Considering that the five models employ the same CA module, the ST-CA produces the most accurate details in the maps of development potential, which reduces both the overestimation and underestimation of LUCC at the same time.

4. Discussion

4.1. Advantages of the ST-CA model

The results demonstrated that the proposed ST-CA model achieved the best accuracy in the LUCC simulation of China among the analyzed models. Theoretically, the improvement can be attributed to the ability of the 3D-CNN in the potential generation module to capture the spatiotemporal neighborhood effects and the nonlinear relationships in the LUCC process.

Neighborhood effects are crucial factors for the calculation of development potentials (He et al., 2018). In our proposed ST-CA model, the spatial and temporal neighborhood effects were simultaneously handled through spatiotemporal convolutions on time-series driving factors. The 3D kernels slide over the data cubes to extract the spatiotemporal features regardless of the priority. Meanwhile, the convolution

Table 2
The FoM and kappa of the simulations.

	LR-CA		RF-CA		FCN-CA		CNN-–CA		ST-CA	
	FoM (%)	Kappa	FoM (%)	Kappa	FoM (%)	Kappa	FoM (%)	Kappa	FoM (%)	Kappa
CC	6.92	0.978	5.63	0.980	13.09	0.983	18.36	0.984	21.70	0.985
EC	7.58	0.981	5.37	0.979	13.52	0.983	18.45	0.984	20.36	0.990
NC	6.72	0.988	5.82	0.989	10.65	0.987	16.16	0.989	18.26	0.989
NE	6.64	0.987	4.23	0.980	12.55	0.988	16.83	0.990	20.86	0.994
NW	7.47	0.985	6.10	0.984	10.75	0.987	15.37	0.980	17.19	0.987
SC	6.82	0.980	5.01	0.979	12.74	0.979	16.56	0.983	17.98	0.983
SW	3.39	0.994	3.03	0.994	9.44	0.994	14.83	0.994	16.49	0.995
Overall	6.77	0.989	5.31	0.989	11.41	0.990	16.13	0.989	18.42	0.991

Table 3
The error (%) of the simulations.

	Arable		Forest		Grass		Water		Construction		Unused		Total
	CE	OE	CE	OE	CE	OE	CE	OE	CE	OE	CE	OE	
LR-CA	1.24	1.08	0.29	0.30	0.50	0.52	3.13	0.91	9.43	9.35	0.31	0.73	0.83
RF-CA	1.39	1.39	0.30	0.29	0.44	0.44	1.87	1.86	9.70	9.69	0.60	0.61	0.88
FCN-CA	1.19	1.17	0.24	0.27	0.51	0.51	1.70	1.65	8.44	7.31	0.44	0.56	0.78
CNN-CA	1.02	0.99	0.23	0.25	0.70	0.76	3.99	3.98	7.43	6.63	0.48	0.47	0.85
ST-CA	1.16	1.25	0.16	0.23	0.47	0.52	1.48	0.81	7.25	6.40	0.48	0.43	0.71

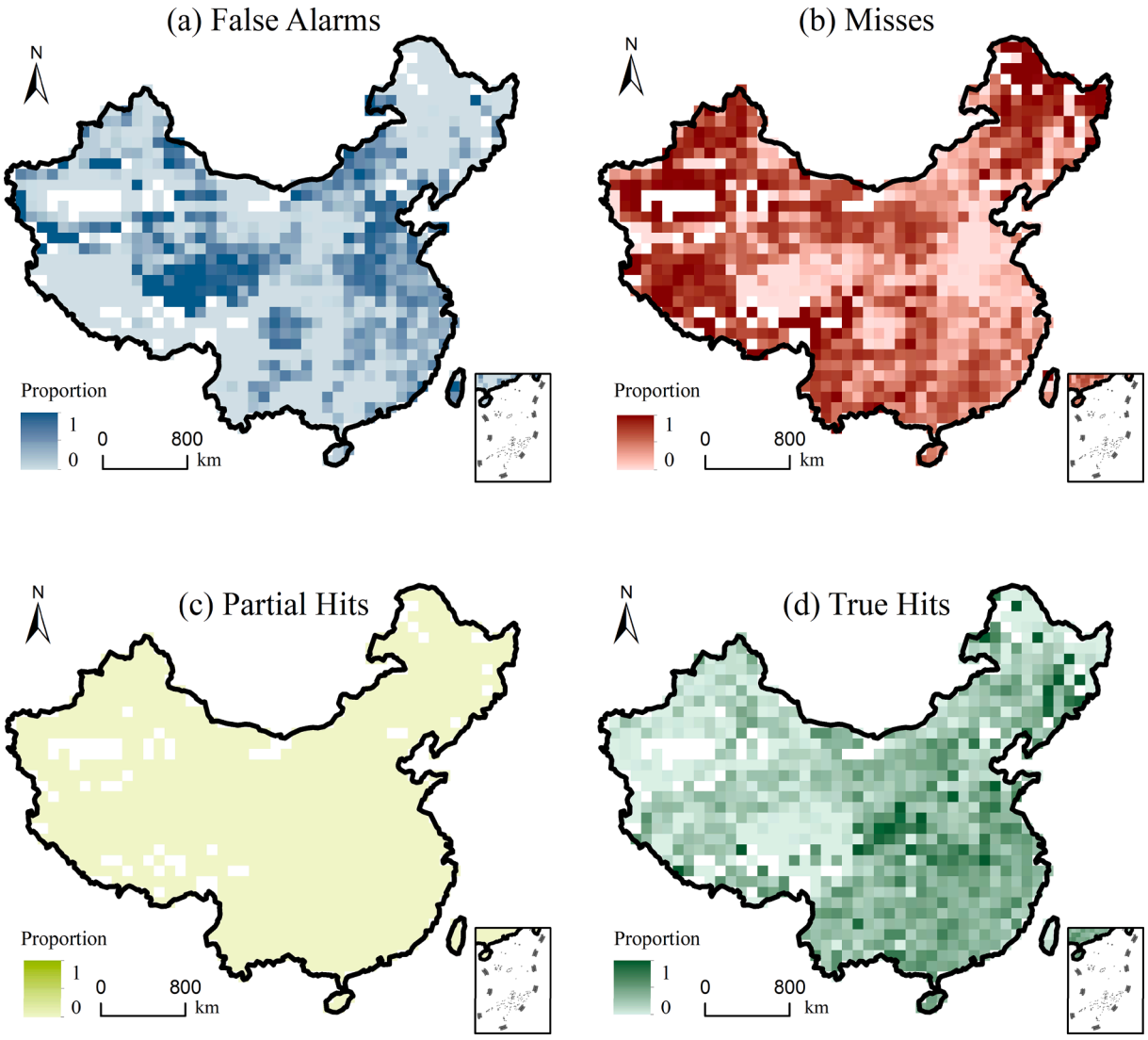

Fig. 8. The spatial distribution of the proportion of pixels that were incorrectly predicted (a), (b), (c) and accurately predicted (d).

layer is adept at extracting local features, which is appropriate for assimilating the spatiotemporal heterogeneity of driving mechanisms from a geographical perspective. The pooling layer ensures the translation and rotation invariance of features (J. Feng et al., 2018; Leonov et al., 2019). In addition, the stacking of the convolution layers is able to deal with the scale effect because the later layer conducts the convolution on multiple neurons of the previous layer. This is analogous to an upscaling procedure that obtains the driving mechanism from smaller scales to larger scales. Thus, the potential generation module is able to understand the complex spatiotemporal process by learning the latent features beyond the grasp of human cognition (J. Feng et al., 2018).

The nonlinear mechanism between land use and driving factors should also be deliberated in LUCC predictions, especially in rapidly developing regions with complex human-land relationships (G. Shi et al., 2018; Yang et al., 2008). Among the developed models in this study, the LR-CA employed a generalized linear model to generate the potentials, ultimately resulting in an inferior simulation accuracy compared to those of the other nonlinear models. Although the RF-CA captures the nonlinear relationship by the voting of several decision trees, it is suspected of oversimplifying the rules of LUCC on an extended scale, thus obtaining a limited simulation accuracy. In the ST-CA model, however, the fully connected layer in the 3D-CNN inherently captures the nonlinear relationships. The abundant neurons connected to the convolution outcomes are capable of interpreting complex nonlinear

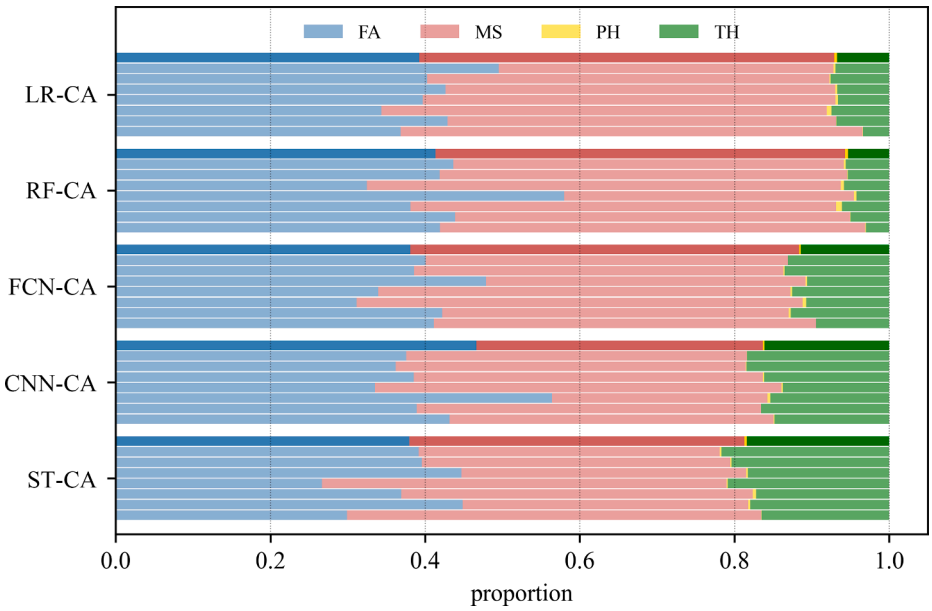

Fig. 9. The proportions of false alarms, misses, partial hits, and true hits.

relationships (Agatonovic-Kustrin & Beresford, 2000), which enables the model to precisely calculate the development potentials of each pixel. In addition, the sufficient samples provided by the large study area also ensure the feasibility of training the network with many parameters. All the strengths above significantly contribute to the LUCC simulation, which is verified by the accuracy comparisons among LR-CA, RF-CA, FCN-CA, CNN-CA, and ST-CA.

4.2. Comparison with existing research

Related studies are introduced to further assess our proposed ST-CA model. The details of each model are collected in Table 4. All these models follow the same structure as ST-CA; in other words, an ML method is applied to calculate the development potentials, and a CA module is applied to conduct spatial allocations. They differ in study areas, resolutions, time spans, and model accuracies. Before comparison, two consensuses should be noted: (1) the FoM value of a long-period simulation is most likely higher than that of a shorter-period simulation (Estoque & Murayama, 2012; Pontius et al., 2008), and (2) the LUCC in large regions with complex climatic conditions and regional differences is more difficult to accurately predict (X. Liu et al., 2017).

Although the FoM of ST-CA is seemingly not as high as those of the other models, our model is still competent when considering its larger spatial scale, shorter time span, better robustness, and wider applications.

Table 4
Model comparison with related studies.

Model	FoM (%)	Study area	Resolution	Time span	Reference
ST-CA*	18.42	Mainland China	1000 *m*	2010–2015	
PLUS (RF + CARS)	22.75	Wuhan, China	30 *m*	2003–2013	(Liang et al., 2021)
FLUS (FCN + CA)	19.62	Mainland China	1000 *m*	2000–2010	(X. Liu et al., 2017)
CNN + VCA	36.10	Shenzhen, China	30 *m*	2009–2012	(Y. Zhai et al., 2020)
CNN + LSTM + CA	40.75	Dongguan, China	80 *m*	2000–2014	(Xing et al., 2020)

PLUS is the model most similar to ST-CA due to the shared CARS module. Although PLUS reached a better FoM of 22.75% in the city-scale simulation of Wuhan (Liang et al., 2021), the employed RF struggles to properly calculate the development potentials for the entire region of China, which has been verified by our comparison experiments.

The FLUS model was applied to the LUCC simulation of China (X. Liu et al., 2017). It achieved an approximately equal FoM to our model even though it employed an FCN that neglected the neighborhood effects. However, the study was conducted based on partitioning of the country. This means that the researchers built disparate models for different regions, which is equivalent to conducting simulations in smaller areas. Additionally, it is intractable for researchers to properly divide a study area into subregions without sufficient prior knowledge (Xia et al., 2019). Our proposed ST-CA model directly simulates the LUCC of China without partitioning and ultimately achieves an approximately equal accuracy. Thus, it obtained better robustness by avoiding the adverse impact of unfaithful compartmentalization and poor data accessibility.

For the model proposed by Zhai, although it employed a CNN to extract neighborhood effects and obtained a satisfying accuracy on the city scale, it can be applied only to binary-state LUCC simulations (e.g., urban vs. nonurban) (Y. Zhai et al., 2020). In contrast, the multiclass simulation conducted by the ST-CA has wider applications to support decision-making.

For the model proposed by Xing, although it employed both the CNN and LSTM to utilize spatiotemporal dependencies (Xing et al., 2020), the smaller study area and the longer time span endowed the model with simplicity to capture the changing pixels. In comparison, our proposed ST-CA model worked well in the spatiotemporal LUCC simulations on a large scale, which involved more complex mechanisms and heterogeneities.

4.3. Limitations and future work

Although the proposed ST-CA model has been proven to achieve superior performance in the LUCC simulation of China on a national scale, there are still some limitations that need to be addressed in future works.

(1) Interpretation of mechanism. ANNs have been widely applied in all areas of research due to their advantages in the accurate simulations of complex processes (Aburas et al., 2019). Once trained, it is usually considered a black box that receives inputs and provides answers. Although the parameters and links in the network indeed reflect the latent relationship between I/O ports, they are hardly comprehended by

humans. Thus, to explicitly interpret the driving mechanism of land conversions, the coupling of a statistical model and a mechanism model is required to better support decision-making.

(2) Adaptive neighborhood. The proposed ST-CA model employs a fixed spatiotemporal window to assimilate the latent features in the whole study area. In fact, however, the precise influential area of neighborhoods is heterogeneous due to the natural and social endowments in different regions (Liao et al., 2016). Thus, an adaptive neighborhood that can automatically identify the proper size of convolution kernels in different regions will be effective to further improve the model accuracy.

(3) Computing expense. The ST-CA model requires more computing resources than traditional models. For instance, it takes 1–2 h to generate the development potentials of China, and the samples also occupy a larger amount of memory. However, this is acceptable in consideration of its higher accuracy along with the booming improvements of computing devices (Lan et al., 2017).

5. Conclusion

LUCC is a nonlinear process containing complex spatiotemporal dependencies that are still challenging to model by existing methods. In this paper, we propose a novel hybrid ST-CA model coupling spatiotemporal property learning and CA-based spatial allocation. A LUCC simulation of China from 2010 to 2015 on a national scale is conducted to test the model performance. The main contributions of this paper can be summarized as follows. (1) Compared to other hybrid LUCC simulation models, the proposed ST-CA model coupling 3D-CNN with CA increased the accuracy of LUCC simulation. (2) Capturing the nonlinear spatiotemporal properties in the simulation process is an effective way to improve LUCC model performance.

Our study is expected to provide a useful tool for policymakers to manage land resources. In future work, we will address the limitations by interpreting the mechanism of land conversion, exploring the adaptive neighborhood, and improving the computational efficiency.

CRediT authorship contribution statement

Jiachen Geng: Conceptualization, Methodology, Data curation, Writing – original draft. **Shi Shen:** Project administration, Methodology, Writing – review & editing. **Changxiu Cheng:** Supervision, Methodology, Funding acquisition, Writing – review & editing. **Kaixuan Dai:** Conceptualization, Data curation.

Declaration of Competing Interest

The authors declare that they have no known competing financial interests or personal relationships that could have appeared to influence the work reported in this paper.

Acknowledgments

This research is funded by National Key Research and Development Plan of China [Grant No. 2019YFA0606901], National Natural Science Foundation of China [Grant No. 42041007], and the Second Tibetan Plateau Scientific Expedition and Research Program (STEP) [Grant No. 2019QZKK0608].

Appendix

A1. Potential maps generated by LR, RF, FCN, and CNN.

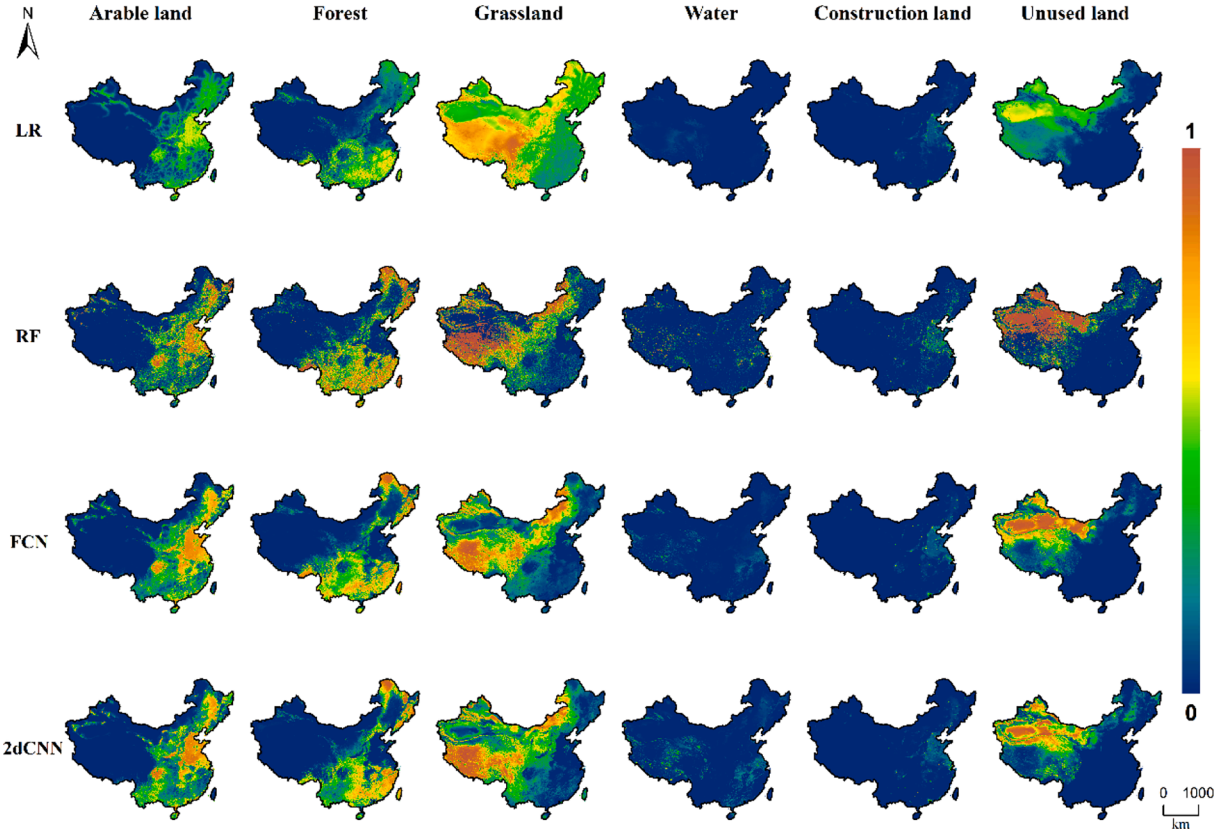

A2. Confusion matrices of the simulations by LR-CA, RF-CA, FCN-CA, CNN-CA, and ST-CA.

(a) Confusion matrix of LR-CA

(b) Confusion matrix of RF-CA

(c) Confusion matrix of FCN-CA

(d) Confusion matrix of CNN-CA

(e) Confusion matrix of ST-CA

References

Aburas, M.M., Ahamad, M.S.S., Omar, N.Q., 2019. Spatio-temporal simulation and prediction of land-use change using conventional and machine learning models: a review. Environ. Monit. Assess. 191 (4) https://doi.org/10.1007/s10661-019-7330-6.

Agatonovic-Kustrin, S., Beresford, R., 2000. Basic concepts of artificial neural network (ANN) modeling and its application in pharmaceutical research. J. Pharm. Biomed. Anal. 22 (5), 717–727. https://doi.org/10.1016/S0731-7085(99)00272-1.

Anurag, Saxena, A., & Pradhan, B. 2018. Land use/land cover change modelling: Issues and challenges. Journal ofof Rural Development, 37(2), 413–424. 10.25175/jrd/2018/v37/i2/129708.

Breiman, L., 2001. Random Forests. Machine Learning 45 (1), 5–32. https://doi.org/10.1023/A:1010933404324.

Cao, C., Dragićević, S., Li, S., 2019. Short-term forecasting of land use change using recurrent neural network models. Sustainability 11 (19), 5376. https://doi.org/10.3390/su11195376.

Cao, K., Huang, B., Wang, S., Lin, H., 2012. Sustainable land use optimization using Boundary-based Fast Genetic Algorithm. Comput. Environ. Urban Syst. 36 (3), 257–269. https://doi.org/10.1016/j.compenvurbsys.2011.08.001.

Cao, M., Tang, G., Shen, Q., Wang, Y., 2015. A new discovery of transition rules for cellular automata by using cuckoo search algorithm. International Journal of Geographical Information Science 29 (5), 806–824. https://doi.org/10.1080/13658816.2014.999245.

Ding, W.J., Wang, R.Q., Wu, D.Q., Liu, J., 2013. Cellular automata model as an intuitive approach to simulate complex land-use changes: An evaluation of two multi-state land-use models in the Yellow River Delta. Stoch. Env. Res. Risk Assess. 27 (4), 899–907. https://doi.org/10.1007/s00477-012-0624-7.

Estoque, R.C., Murayama, Y., 2012. Examining the potential impact of land use / cover changes on the ecosystem services of Baguio city, the Philippines: A scenario-based analysis. Appl. Geogr. 35 (1–2), 316–326. https://doi.org/10.1016/j.apgeog.2012.08.006.

Feng, J., Liu, J., Pan, C., 2018. Complex Behavior Recognition Based on Convolutional Neural Network: A Survey. In: 2018 14th International Conference on Mobile Ad-Hoc and Sensor Networks (MSN), pp. 103–108. https://doi.org/10.1109/MSN.2018.00024.

Feng, Y., Tong, X., 2018. Dynamic land use change simulation using cellular automata with spatially nonstationary transition rules. GIScience and Remote Sensing 55 (5), 678–698. https://doi.org/10.1080/15481603.2018.1426262.

Gharaibeh, A., Shaamala, A., Obeidat, R., Al-Kofahi, S., 2020. Improving land-use change modeling by integrating ANN with Cellular Automata-Markov Chain model. Heliyon 6 (9), e05092. https://doi.org/10.1016/j.heliyon.2020.e05092.

Gounaridis, D., Chorianopoulos, I., Symeonakis, E., Koukoulas, S., 2019. A Random Forest-Cellular Automata modelling approach to explore future land use/cover change in Attica (Greece), under different socio-economic realities and scales. Sci. Total Environ. 646, 320–335. https://doi.org/10.1016/j.scitotenv.2018.07.302.

Grekousis, G., 2019. Artificial neural networks and deep learning in urban geography: A systematic review and meta-analysis. Comput. Environ. Urban Syst. 74, 244–256.

He, J., Li, X., Yao, Y., Hong, Y., Jinbao, Z., 2018. Mining transition rules of cellular automata for simulating urban expansion by using the deep learning techniques. International Journal of Geographical Information Science 32 (10), 2076–2097. https://doi.org/10.1080/13658816.2018.1480783.

Houghton, R.A., Nassikas, A.A., 2017. Global and regional fluxes of carbon from land use and land cover change 1850–2015. Global Biogeochem. Cycles 31 (3), 456–472. https://doi.org/10.1002/2016GB005546.

Ji, S., Xu, W., Yang, M., Yu, K., 2013. 3D Convolutional neural networks for human action recognition. IEEE Trans. Pattern Anal. Mach. Intell. 35 (1), 221–231. https://doi.org/10.1109/TPAMI.2012.59.

Ju, H., Zhang, Z., Zuo, L., Wang, J., Zhang, S., Wang, X., Zhao, X., 2016. Driving forces and their interactions of built-up land expansion based on the geographical detector - a case study of Beijing, Chinaudy of Beijing, China. International Journal of Geographical Information Science 30 (11), 2188–2207. https://doi.org/10.1080/13658816.2016.1165228.

Kourosh Niya, A., Huang, J., Kazemzadeh-Zow, A., Karimi, H., Keshtkar, H., Naimi, B., 2020. Comparison of three hybrid models to simulate land use changes: A case study in Qeshm Island. Iran. *Environmental Monitoring and Assessment* 192 (5), 302. https://doi.org/10.1007/s10661-020-08274-6.

Lan, Q., Wang, Z., Wen, M., Zhang, C., Wang, Y., 2017. High performance implementation of 3D convolutional neural networks on a GPU. Computational Intelligence and Neuroscience 2017, 1–8. https://doi.org/10.1155/2017/8348671.

Leonov, S. C., Vasilyev, A. N., Makovetskii, A., & Vitaly, K. 2019. Analysis of the convolutional neural network architectures in image classification problems. In A. G. Tescher & T. Ebrahimi (Eds.), *Applications of Digital Image Processing XLII*. SPIE. 10.1117/12.2529232.

Li, C., Yang, M., Li, Z., Wang, B., 2021. How will Rwandan land use/land cover change under high population pressure and changing climate? Applied Sciences (Switzerland) 11 (12). https://doi.org/10.3390/app11125376.

Li, G., Zhang, F., Jing, Y., Liu, Y., Sun, G., 2017a. Response of evapotranspiration to changes in land use and land cover and climate in China during 2001–2013. Sci. Total Environ. 596, 256–265. https://doi.org/10.1016/j.scitotenv.2017.04.080.

Li, S., Liu, X., Li, X., Chen, Y., 2017b. Simulation model of land use dynamics and application: Progress and prospects. Journal of Remote Sensing 21 (3), 329–340.

Liang, X., Guan, Q., Clarke, K.C., Liu, S., Wang, B., Yao, Y., 2021. Understanding the drivers of sustainable land expansion using a patch-generating land use simulation (PLUS) model: A case study in Wuhan, China. Comput. Environ. Urban Syst. 85, 101569. https://doi.org/10.1016/j.compenvurbsys.2020.101569.

Liao, J., Tang, L., Shao, G., Su, X., Chen, D., Xu, T., 2016. Incorporation of extended neighborhood mechanisms and its impact on urban land-use cellular automata simulations. Environ. Modell. Software 75, 163–175. https://doi.org/10.1016/j.envsoft.2015.10.014.

Liu, J., Kuang, W., Zhang, Z., Xu, X., Qin, Y., Ning, J., Zhou, W., Zhang, S., Li, R., Yan, C., Wu, S., Shi, X., Jiang, N., Yu, D., Pan, X., Chi, W., 2014a. Spatiotemporal characteristics, patterns, and causes of land-use changes in China since the late 1980s. J. Geog. Sci. 24 (2), 195–210. https://doi.org/10.1007/s11442-014-1082-6.

Liu, X., Hu, G., Ai, B., Li, X., Tian, G., Chen, Y., Li, S., 2018. Simulating urban dynamics in China using a gradient cellular automata model based on S-shaped curve evolution characteristics. International Journal of Geographical Information Science 32 (1), 73–101. https://doi.org/10.1080/13658816.2017.1376065.

Liu, X., Liang, X., Li, X., Xu, X., Ou, J., Chen, Y., Li, S., Wang, S., Pei, F., 2017. A future land use simulation model (FLUS) for simulating multiple land use scenarios by coupling human and natural effects. Landscape Urban Plann. 168 (October), 94–116. https://doi.org/10.1016/j.landurbplan.2017.09.019.

Liu, Y., Fang, F., Li, Y., 2014b. Key issues of land use in China and implications for policy making. Land Use Policy 40, 6–12. https://doi.org/10.1016/j.landusepol.2013.03.013.

Ma, Z., Xu, Y., Peng, J., Chen, Q., Wan, D., He, K., Shi, Z., Li, H., 2018. Spatial and temporal precipitation patterns characterized by TRMM TMPA over the Qinghai-Tibetan plateau and surroundings. Int. J. Remote Sens. 39 (12), 3891–3907. https://doi.org/10.1080/01431161.2018.1441565.

Milad, M., Ming, Y., Firuz, M., Hanan, Z., 2016. The simulation and prediction of spatio-temporal urban growth trends using cellular automata models: A review. Int. J. Appl. Earth Obs. Geoinf. 52, 380–389. https://doi.org/10.1016/j.jag.2016.07.007.

Mishra, V.N., Rai, P.K., Prasad, R., Punia, M., Nistor, M., 2018. Prediction of spatio-temporal land use/land cover dynamics in rapidly developing Varanasi district of Uttar Pradesh, India, using geospatial approach: A comparison of hybrid models. Applied Geomatics 10 (3), 257–276. https://doi.org/10.1007/s12518-018-0223-5.

Mustafa, A., Cools, M., Saadi, I., Teller, J., 2017. Coupling agent-based, cellular automata and logistic regression into a hybrid urban expansion model (HUEM). Land Use Policy 69, 529–540. https://doi.org/10.1016/j.landusepol.2017.10.009.

Mustafa, A., Rienow, A., Saadi, I., Cools, M., Teller, J., 2018. Comparing support vector machines with logistic regression for calibrating cellular automata land use change models. European Journal of Remote Sensing 51 (1), 391–401. https://doi.org/10.1080/22797254.2018.1442179.

Pontius, R.G., Boersma, W., Castella, J.-C., Clarke, K., de Nijs, T., Dietzel, C., Duan, Z., Fotsing, E., Goldstein, N., Kok, K., Koomen, E., Lippitt, C.D., McConnell, W., Mohd Sood, A., Pijanowski, B., Pithadia, S., Sweeney, S., Trung, T.N., Veldkamp, A.T., Verburg, P.H., 2008. Comparing the input, output, and validation maps for several models of land change. Annals of Regional Science 42 (1), 11–37. https://doi.org/10.1007/s00168-007-0138-2.

Rahman, M.T.U., Esha, E.J., 2020. Prediction of land cover change based on CA-ANN model to assess its local impacts on Bagerhat, southwestern coastal Bangladesh. Geocarto International 1–23. https://doi.org/10.1080/10106049.2020.1831621.

Ren, Y., Lü, Y., Comber, A., Fu, B., Harris, P., Wu, L., 2019. Spatially explicit simulation of land use/land cover changes: Current coverage and future prospects. Earth Sci. Rev. 190 (March), 398–415. https://doi.org/10.1016/j.earscirev.2019.01.001.

Rienow, A., Goetzke, R., 2015. Supporting SLEUTH - Enhancing a cellular automaton with support vector machines for urban growth modeling. Comput. Environ. Urban Syst. 49, 66–81. https://doi.org/10.1016/j.compenvurbsys.2014.05.001.

Sankarrao, L., Ghose, D.K., Rathinsamy, M., 2021. Predicting land-use change: Intercomparison of different hybrid machine learning models. Environ. Modell. Software 145, 105207. https://doi.org/10.1016/j.envsoft.2021.105207.

Sante, I., Garcia, A.M., Miranda, D., Crecente, R., 2010. Cellular automata models for the simulation of real-world urban processes: A review and analysis. Landscape Urban Plann. 96 (2), 108–122. https://doi.org/10.1016/j.landurbplan.2010.03.001.

Schulp, C.J.E., Nabuurs, G.J., Verburg, P.H., 2008. Future carbon sequestration in Europe-Effects of land use change. Agric. Ecosyst. Environ. 127 (3–4), 251–264. https://doi.org/10.1016/j.agee.2008.04.010.

Shafizadeh-Moghadam, H., Minaei, M., Feng, Y., Pontius, R.G., 2019. GlobeLand30 maps show four times larger gross than net land change from 2000 to 2010 in Asia. Int. J. Appl. Earth Obs. Geoinf. 78, 240–248. https://doi.org/10.1016/j.jag.2019.01.003.

Shafizadeh-Moghadam, H., Tayyebi, A., Helbich, M., 2017. Transition index maps for urban growth simulation: application of artificial neural networks, weight of evidence and fuzzy multi-criteria evaluation. Environ. Monit. Assess. 189 (6) https://doi.org/10.1007/s10661-017-5986-3.

Shi, G., Jiang, N., Yao, L., 2018. Land Use and Cover Change during the Rapid Economic Growth Period from 1990 to 2010: A Case Study of Shanghai. Sustainability 10 (2), 426. https://doi.org/10.3390/su10020426.

Shi, M., Wu, H., Fan, X., Jia, H., Dong, T., He, P., Baqa, M.F., Jiang, P., 2021. Trade-offs and synergies of multiple ecosystem services for different land use scenarios in the yili river valley, china. Sustainability 13 (3), 1577. https://doi.org/10.3390/su13031577.

Sidharthan, R., Bhat, C.R., 2012. Incorporating Spatial Dynamics and Temporal Dependency in Land Use Change Models. Geographical Analysis 44 (4), 321–349. https://doi.org/10.1111/j.1538-4632.2012.00854.x.

Tobler, W., 1970. A Computer Movie Simulating Urban Growth in the Detroit Region. Economic Geography 46 (2), 234–240. https://doi.org/10.2307/143141.

Tran, D., Bourdev, L., Fergus, R., Torresani, L., Paluri, M., 2015. Learning spatiotemporal features with 3D convolutional networks. In: Proceedings of the IEEE International Conference on Computer Vision. https://doi.org/10.1109/ICCV.2015.510.

Vani, M., Prasad, P.R.C., 2021. Modelling urban expansion of a south-east Asian city, India: Comparison between SLEUTH and a hybrid CA model. In: Modeling Earth Systems and Environment. https://doi.org/10.1007/s40808-021-01150-3.

Verburg, P.H., Schot, P.P., Dijst, M.J., Veldkamp, A., 2004. Land use change modelling: Current practice and research priorities. GeoJournal 61 (4), 309–324. https://doi.org/10.1007/s10708-004-4946-y.

Xia, C., Zhang, A., Wang, H., Zhang, B., 2019. Modeling urban growth in a metropolitan area based on bidirectional flows, an improved gravitational field model, and partitioned cellular automata. International Journal of Geographical Information Science 33 (5), 877–899. https://doi.org/10.1080/13658816.2018.1562067.

Xing, W., Qian, Y., Guan, X., Yang, T., Wu, H., 2020. A novel cellular automata model integrated with deep learning for dynamic spatio-temporal land use change simulation. Computers and Geosciences 137, 104430. https://doi.org/10.1016/j.cageo.2020.104430.

Yang, Q., Li, X., Shi, X., 2008. Cellular automata for simulating land use changes based on support vector machines. Comput. Geosci. 34 (6), 592–602. https://doi.org/10.1016/j.cageo.2007.08.003.

Yao, Y., Liu, X., Li, X., Liu, P., Hong, Y., Zhang, Y., Mai, K., 2017. Simulating urban land-use changes at a large scale by integrating dynamic land parcel subdivision and vector-based cellular automata. International Journal of Geographical Information Science 31 (12), 2452–2479. https://doi.org/10.1080/13658816.2017.1360494.

Zhai, H., Lv, C., Liu, W., Yang, C., Fan, D., Wang, Z., & Guan, Q. 2021. Understanding Spatio-Temporal Patterns of Land Use/Land Cover Change under Urbanization in Wuhan, China, 2000–2019. *Remote Sensing*, *13*(16). 10.3390/rs13163331.

Zhai, Y., Yao, Y., Guan, Q., Liang, X., Li, X., Pan, Y., Yue, H., Yuan, Z., Zhou, J., 2020. Simulating urban land use change by integrating a convolutional neural network with vector-based cellular automata. International Journal of Geographical Information Science 34 (7), 1475–1499. https://doi.org/10.1080/13658816.2020.1711915.